Journal of Molecular Liquids 364 (2022) 119967

Contents lists available at ScienceDirect

Journal of Molecular Liquids

journal homepage: www.elsevier.com/locate/molliq

Adsorption properties of graphene materials for pesticides: Structure effect

Xuejuan Shi [a,1], Caihong Cheng [b,c,1], Fei Peng [b,c], Wenlong Hou [b,c], Xiaohu Lin [b], Xiuping Wang [a,b,*]

[a] Hebei Key Laboratory of Crop Stress Biology (in preparation), College of Agronomy and Biotechnology, Hebei Normal University of Science and Technology, Qinhuangdao 066000, PR China
[b] Analysis and Testing Center, Hebei Normal University of Science and Technology, Qinhuangdao 066000, PR China
[c] Hebei Key Laboratory of Active Components and Functions in Natural Products, Hebei Normal University of Science and Technology, Qinhuangdao 066004, PR China

ARTICLE INFO

Article history:
Received 27 January 2022
Revised 19 July 2022
Accepted 26 July 2022
Available online 30 July 2022

Keywords:
Graphene materials
Pesticides
Adsorption
Structure effect
Multi-mechanisms
Response surface methodology

ABSTRACT

In recent years, the application of graphene materials to the adsorption of pesticides has attracted great research interests. However, to the best of our knowledge, there has been no report about the specific adsorption mechanism of graphene materials for pesticides with different structures. This study investigated the potential adsorption mechanism of graphene oxide (GO) and reduced graphene oxide (rGO) for three pesticides with different structures [Methomyl (Met; without aromatic rings), Acetamiprid (Ace; one aromatic ring) and Azoxystrobin (Azo, three aromatic rings)]. The operating variables including time, temperature and initial pesticide concentration were estimated and optimized with face-centered composite design (FCCD) through response surface methodology (RSM). Under optimal conditions, the calculated adsorption capacity of GO for Met, Ace and Azo was 106.22, 285.96 and 2896.84 mg/g; while that of rGO was 96.86, 357.65 and 2818.04 mg/g, respectively. The adsorption kinetics follows the pseudo second-order and Elovich models, while the adsorption isotherm can be well described by the Sips model. Thermodynamic study revealed that the adsorption process of the three pesticides onto GO or rGO was an exothermic and physical process. The adsorption was deduced to be synergistically driven by (1) the π-π conjugation between the sp^2 region of adsorbent and the aromatic ring of pesticide molecules, (2) H-bonding and electrostatic interaction between heteroatoms in pesticide molecules and oxygen-containing functional groups on adsorption materials, and (3) H-bonding and π-π conjugation between pesticides. In general, this study provides important practical and theoretical implications for understanding the molecular mechanism underlying the adsorption of pollutants by GO or rGO and its practical application.

1. Introduction

Pesticides are widely applied to the protection of crops from insects, diseases and weeds to for quality control and management in production. It has been reported that nearly two million tons of pesticides are consumed every year to control pests worldwide, among which 45%, 25% and 25% are used in Europe, USA and the rest of the world, respectively [1]. Generally, the effective utilization rate of pesticides is lower than 10%, while over 90% of the applied pesticides fail to exert any bioactivity due to degradation, volatilization and leaching into the environment [2]. Undoubtedly, pesticides easily cause serious water and soil contaminations due their low utilization rate and poor biodegradability, posing serious threats to the ecosystems and human health [3–7]. Currently, detection and elimination of pesticides from ecosystems are a critical issues for the protection of environment [8].

Water safety, which is essential for all living organisms, is closely related to human activities [9]. Pesticides in water bodies are mainly derived from diffuse and point sources, particularly the diffuse source [10]. Various strategies have been applied to the removal of pesticide molecules from aqueous environments, such as bioremediation, advanced oxidation processes (AOPs), adsorption and photo catalytic degradation [11–16]. Among these commonly used strategies, adsorption has notable advantages such as simple operation, high efficiency, abundant source and low cost. So far, adsorbents for pesticide removal, such as activated carbon,

* Corresponding author at: Analysis and Testing Center, Hebei Normal University of Science and Technology, No.360 west section of Hebei street, Qinhuangdao 066000, Hebei Provence, PR China.
E-mail address: wangxiuping0721@163.com (X. Wang).
[1] These two authors contributed equally.

https://doi.org/10.1016/j.molliq.2022.119967
0167-7322/

multi-walled carbon nanotubes, biochars and polymers, have been widely reported [17–20].

Currently, graphene-based materiasl have been introduced as a renewable materials with low secondary pollution and high adsorption performance for pesticide adsorption removal from wastewaters, which has attracted great research interests due to the high stability, large specific surface area, rich sp^2 bonding, abundant oxygen functional groups and large delocalized π-π electrons [21,22]. For example, Nodeh et al. suggested that magnetic graphene oxide (GO) can achieve high adsorption capacities for chlorpyrifos (78.74 mg g^{-1}) and hexaconazole (93.46 mg g^{-1}) [23]. Moreover, GO/SiO_2 composite can remove herbicide paraquat from aqueous solutions with a a high adsorption capacity (31.34 mg g^{-1}) when used as an adsorbent [24]. Although numerous studies have demonstrated the high adsorption capacities of GO for pesticides, the underlying molecular mechanism remains largely unknown. Particularly, the molecular mechanism underlying the adsorption of GO or reduced GO (rGO) for pesticides may vary with different pesticide structures.

In this work, three pesticides with different structures [Methomyl (Met; without aromatic rings), Acetamiprid (Ace; one aromatic ring) and Azoxystrobin (Azo; three aromatic rings)] were used to study the molecular mechanism for the adsorption of pesticides by GO and rGO. The structure information of the three pesticides is shown in Table S1. The adsorbent was characterized by FT-IR, TGA, Raman and XPS. The mechanism for the adsorption of the three pesticides by GO/rGO was dissected based on adsorption kinetics, adsorption isotherms and thermodynamics combined with SEM and FT-IR. Understanding the interaction between the GO/rGO surface and target pollutants and the microscopic adsorption mechanism may be of great theoretical and practical significance for the treatment of polluted water on a large scale.

2. Experimental

2.1. Materials

All chemicals were of analytical grade and used without further purification. Certified reference materials of Met and Azo were obtained from Shanghai Pesticide Research Institute (Shanghai, China). Ace was purchased from Beijing North Weiye Measurement Technology Research Institute (Beijing, China). Graphite was provided by Qingdao Tianhe Graphite Co. Ltd., whose average particle diameter was 4 mm (99.95% purity). Concentrated sulfuric acid (H_2SO_4) and hydrochloric acid (HCl) were provided by Tianjin No.3 Chemical Plant. Hydrazine hydrate was obtained from Tokyo Chemical Industry Co. Ltd.

2.2. Preparation and Characterization of GO and rGO

GO was synthesized in reference to the modified Hummers method described in our previous study [25]. Briefly, natural graphite powder was added into H_2SO_4 solution for the production of graphite oxide (GtO). Then, the GtO sample was filtered and washed with HCl (10% v/v) and deionized water (DI) for the removal of chemical residues, which was then subjected to centrifugal washing until neutrality so as to remove unexfoliated GO. Then, the GO was suspended in DI under strong stirring and ultrasonication for at least 1 h to synthesize rGO. The reduction was performed with hydrazine hydrate (the hydrazine hydrate/GO weight ratio = 10) at 95 °C. Stirring and intermittent ultrasonication were provided throughout the whole preparation process. After completion, the rGO powder was immediately isolated via filtration, and washed with distilled water for four times, followed by drying at 40 °C to remove the residual solvent [26]. The synthetic routes for GO and rGO are shown in Fig. 1.

Fourier-transform infrared spectroscopy (FT-IR, BrukerTensor27, Germany) of GO and rGO was used to identify the variations of functional groups. Thermo-gravimetric analysis (TGA, Netzsch STA 409PCLuxx, Germany) was conducted at 25–800℃ with the rate of 10℃/min in an N_2 atmosphere. Raman spectra were captured using a Raman spectrometer (Horiba HR-800, France). X-ray photoelectron spectroscopy (XPS, Thermo fisher Scientific K-Alpha+, USA) was used for the quantitative analysis of the surface elements in the samples. The data were analyzed with the XPS Avantage 5.52 software. The morphology and structure of the samples were captured by scanning electron microscopy (SEM, Hitachi SU8010, Japan). The zeta potential measurement was performed using the Zetasizer Nano-ZS90 System (Malvern Inc.).

2.3. Adsorption experiments

Batch adsorption kinetics experiments of Met, Ace and Azo onto the surface of GO and rGO were carried out. In each test, 1 mg of each adsorbent (GO and rGO) was mixed with 20 mL of 50 mg/L pesticides solutions in a 50 mL centrifuge tube at 298 K, and the pesticides were analyzed at time intervals of 0.5, 1, 1.5, 2, 2.5, 3, 4, 5, 6, 7, 8 and 9 h after the adsorption experiments. The adsorption isotherm experiments were performed in the same way as the adsorption kinetics experiment at 298 K. The initial concentrations of Met, Ace and Azo ranged from 5 to 100 mg/L, 5 to 150 mg/L and 50 to 300 mg/L, respectively. Experiments for adsorption thermodynamics were conducted with the addition of 1 mg of adsorbent into pesticide solutions (20 mL, 50 mg/L) at the temperature of 298, 308 and 318 K.

All the above experiments were conducted in triplicates and under shaking at 200 rpm for 9 h to achieve adsorption equilibrium. All aqueous phases in the mixture were separated from the adsorbent through 1 min of centrifugation at 14000 rpm and filtering of the supernatant through a 0.45 μm membrane filter before analysis. The pesticide concentration in the samples was measured with a high performance liquid chromatography (HPLC) system (UltiMate 3000, Thermo Fisher Scientific, USA). The information about the standard curve of the three pesticides is presented in Table S2.

The adsorption capacity of each adsorbent was calculated with Eq. (1):

$$Q_t = (C_0 - C_t) * v/m$$

where Q_t represents the adsorption capacity of the adsorbent (mg/g), V is the sample volume of the pesticide (L), m indicates the adsorbent dosage (g), C_0 stands for the initial concentration of the pesticide (mg/L) and C_t is the residual concentration of the pesticide at time t (mg /L).

2.4. Adsorption kinetic model

The kinetic models could be used to ascertain the relationship between adsorption time and adsorption capacity and analyze the adsorption mechanism of pesticides on GO and rGO [27]. Thus, the pseudo first-order [Eq. (2)], pseudo second-order [Eq. (3)], and Elovich [Eq. (4)] were used to fit the kinetic experiments data in this study [19,28].

$$Q_t = Q_e(1 - e^{-K_1 t} \quad (2)$$

$$Q_t = Q_e^2 K_2 t/(1 + K_2 Q_e t) \quad (3)$$

$$Q_t = (1/\beta) * ln(1 + \alpha\beta t) \quad (4)$$

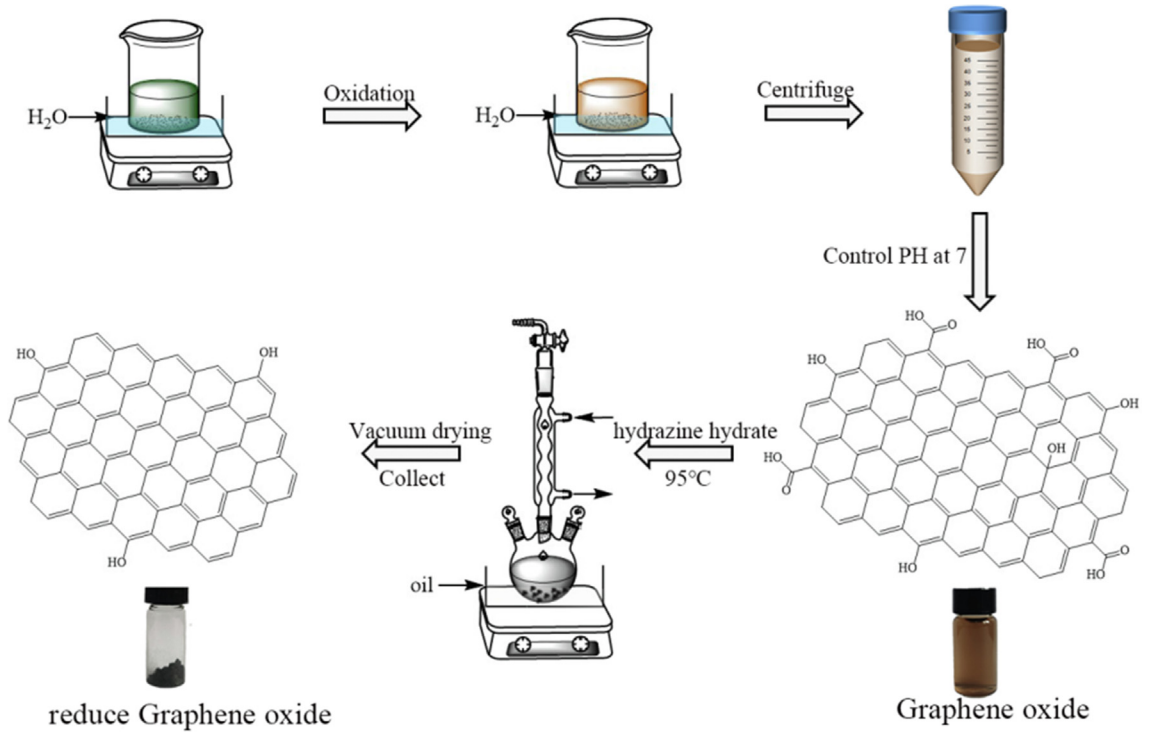

Fig. 1. Synthetic routes for the fabrication of GO and rGO.

where Q_t is the adsorption capacity of the adsorbent at time t (mg/g), Q_e indicates the adsorption capacity of the adsorbent at equilibrium (mg/g), K_1 represents the kinetic rate constant (1/h) of the pseudo first-order, K_2 is the kinetic rate constant [g/(mg·h)] of the pseudo second-order, α represents the initial adsorption rate (mg/g), β indicates the desorption constant (g/mg) and t is the adsorption time (h).

2.5. Adsorption isotherm model

The absorption isotherm model could be employed to analyze the adsorption mechanism of pesticides on GO and rGO. The experimental data of adsorption isotherm were fitted into five isotherm models, namely Langmuir, Freundlich, Temkin, Dubinin–Radushkevich and Sips. Eq. (5) shows the Langmuir isotherm model that can be expressed as follows [29]:

$$Q_e = Q^0_{max} K_L C_e / (1 + K_L C_e) \tag{5}$$

where Q_e indicates the adsorption capacity of the adsorbent at equilibrium (mg/g), C_e indicates the adsorbate concentration at equilibrium (mg/L), Q^0_{max} represents the maximum saturated monolayer adsorption capacity of adsorbent (mg/g), and K_L is a constant related to the affinity between an adsorbent and adsorbate (L/mg). The Freundlich isotherm [Eq. (6)] can be shown as follows [30]:

$$Q_e = K_F C_e^n \tag{6}$$

where K_F is the Freundlich constant (mg/g)/(mg/L)^n and n (dimensionless) is the Freundlich intensity parameter, which indicates the magnitude of the adsorption driving force or the surface heterogeneity. The heat of adsorption can be represented by Temkin isotherm [Eq. (7)] [31,32].

$$Q_e = (RT/b_T) * \ln A_T C_e \tag{7}$$

where R is the gas constant [0.008314 kJ/(mol·K)], T indicates the temperature (K), A_T is the Temkin isotherm binding constant (L/mg) and b_T is a constant corresponding to the heat of absorption (kJ/mol). Eqs. (8) and (9) describe the Dubinin-Radushkevich isotherm model [33]:

$$Q_e = q_{DR} e^{-K_{DR}\varepsilon^2} \tag{8}$$

$$\varepsilon = RT ln[1 + (1/C_e)] \tag{9}$$

$$E = 1/\sqrt{2K_{DR}} \tag{10}$$

where q_{DR} is the theoretical adsorption capacity (mg/g), K_{DR} indicates a constant related to the absorption energy (mol^2/kJ^2) and ε is the Polanyi potential. Eq. (10) expresses the free energy (E) of adsorption (kJ/mol), which can be used to indicate the mechanism of absorption process. The Sips isotherm [Eq. (11)] is represented as follows [34]:

$$Q_e = K_s C_e^{b_s} / \left(1 + a_s C_e^{b_s}\right) \tag{11}$$

where K_s is the Sips model isotherm constant (L/mg), a_s represents the Sips model constant and b_s is the Sips model exponent.

2.6. Adsorption thermodynamics

The absorption thermodynamic calculation was carried out with the Van't Hoff equation [Eqs. (12)–(14)].

$$\ln K_c = \Delta S/R - \Delta H/RT \tag{12}$$

$$\Delta G = -RT \ln K_c \tag{13}$$

$$\Delta G = \Delta H - T\Delta S \tag{14}$$

where R is the gas constant (0.008314 kJ/(mol·K)), T represents the temperature (K), ΔH indicates the variation in enthalpy (kJ/mol), ΔS is the variation in entropy [kJ/(mol·K)] and ΔG is the variation in

Gibbs free energy (kJ/mol). K_c is the thermodynamic equilibrium constant and can be obtained with $K_c = Q_e/C_e$ [35].

2.7. Experimental design

A face-centered composite design (FCCD) was employed to estimate and optimize of the independent variables (time, temperature and initial pesticide concentration) on the adsorption efficiency of three pesticides by GO and rGO [36]. Table 1 shows the values of the independent variables and the coding levels in the adsorption experiments of Met onto GO and rGO, and others are presented in Tables S3 and S4. Twenty experiments were considered as calculated from Eq. (15) [37].

$N = 2^{k} + 2k + n_c$ (15).where k is the number of factors, n_c used for predicting the residual error is the replicates in central points.

For estimating the optimal conditions, the quadratic equation model was presented in Eq. (16).

$$Y = \beta_0 + \sum_{i=1}^{k} \beta_i x_i + \sum_{i=1}^{k} \beta_{ii} x_{ii}^2 + \sum_{i=1}^{k-1} \sum_{j=i+1}^{k} \beta_{ij} x_i x_j + \varepsilon \quad (16)$$

where Y is the response, β_0 is the constant coefficient, β_i, β_{ii}, β_{ij} are coefficients for the linear, quadratic and interaction effect, x_i and x_j are factors, ε is error.

Analysis of variance (ANOVA) was conducted at a 95% significance level to confirm which factors significantly affect the response. The accuracy and applicability of the predicted model were evaluated by the P-values, correlation coefficient (R^2) value, F-test value and lack-of-fit value. The validated model can be plotted in a form of three-dimensional graph to generate surface response for the determination of the best operation conditions.

2.8. Statistical analysis

All the adsorption kinetics and adsorption isothermal experimental data were calculated by SPSS statistical software and the model curve was fit and plotted by Origin 9.0. The surface response experiments were designed and performed, and then the results were analyzed by Design Expert Version 8.0.6.

3. Results and discussion

3.1. Characterization of GO and rGO

The FT-IR spectra of GO and rGO were acquired to observe the chemical composition (Fig. 2a). For pure GO, its characteristic absorption peak at 3356 cm^{-1} corresponds to the C—OH vibration. The peaks at 1720, 1616 and 1375 cm^{-1} are assigned to the vibration of the C=O group, the skeletal vibration of the C—C bond and the O—C—O bond of the carboxyl group, respectively. In addition, the peaks at 1224 and 1051 cm^{-1} are related to the C–O stretching of the epoxy and alkoxy groups, respectively [38,39]. After the reduction of GO, the matrix spectrum of the obtained rGO showed an obvious blue shift. The intensity of the broad band at 3433 cm^{-1} decreased obviously and the peak of the C=O band almost disappeared. However, new peaks appeared at 2924 and 1550 cm^{-1}, which correspond to the vibration of the C—H group and C=C group bending [40,41]. These results further confirmed the substantial removal of oxygen functional groups from GO after the reduction.

The TGA was used to investigate the thermal stability of GO and rGO as illustrated in Fig. 2b. The weight loss of GO in the temperature range of 0–100 ℃ could be ascribed to the removal of physically absorbed water on GO surface. The decomposition of GO at 150–250℃ might be attributed to the degradation of unstable oxygen-containing functional groups including carboxyl, hydroxyl and epoxide groups, which resulted in the generation of gases including steam, CO and CO_2 [42]. Compared with GO, rGO exhibited a higher thermal stability, and there was only a slight mass loss below 700℃, demonstrating the removal of most oxygen-containing functional groups by hydrazine hydrate [26].

Table 1
Independent variables and the coding levels in the adsorption experiments of Met onto GO and rGO.

Independent variables	Coded Levels		
	(−1)	(0)	(+1)
Time (h, X_1)	0.5	1	3
Temperature (°C, X_2)	25	35	45
Met concentration (mg/L, X_3)	10	50	100

Raman spectroscopy was employed to specify the defects and disordered structures of GO and rGO. As shown in Fig. 2c, the Raman spectrum of GO includes a broad band at 1361 cm^{-1}, which is attributed to the breathing mode of the sp2 backbone induced by defects. The absorption band at 1594 cm^{-1} corresponds to the first-order scattering of the E2g mode, which could be definitely assigned to the zone-center LO phonon mode of the lattice [43,44]. However, the Raman spectrum of the rGO sample shows an obvious blue shift relative to that of GO, possibly due to the strong reduction effect. The D to G band intensity ratio (I_D/I_G) is indicative of the crystalline extent of graphene-based materials. As reported in the literature the I_D/I_G ratio was about 1.15 for GO while 1.28 for rGO, indicating that rGO has certain structural defects [26].

To further identify the surface composition, GO and rGO were analyzed with the XPS spectra (Fig. 2d). The results suggested the presence of C1s and O1s on the surface of both GO and rGO. Fig. 2e demonstrates the high-resolution XPS spectra for C1s peaks of GO and rGO and their deconvolution peaks. XPS analysis revealed that the C element usually existed in four chemical states, including C=C (284.7 eV), C—O (285.3 eV), C—O—C/C=O (286.4 eV), and O—C=O (288.3 eV) [45,46]. The C/O ratio was 2.16 and 8.12 for GO and rGO, respectively. The lower C/O ratio of GO indicated the presence of oxygen functional groups, such as hydroxyl, carboxyl, carbonyl and epoxide on the surface of GO, which is in agreement with the results of FT-IR and TGA [47].

The zeta potential of GO and rGO was tested, which is an indirect measure of the surface charge present (Fig. 3). It can be seen that GO exhibited a high negative value of zeta potential (−37 mV) which is attributed to the deprotonation of the oxygen-containing functional groups grafted on the surface of GO such as hydroxyl (—OH) and carboxyl (—COOH) [48]. On the other hand, the zeta potential value on the surface of rGO was −31 mV. Due to the reduction process, the oxygen-containing functional groups on the surface of GO were reduced, resulting in lower negative potential of rGO.

3.2. Adsorption capacity of the adsorbent

Pre-experiments have studied the parameters affecting the adsorption performance, such as pH, the adsorbent dose and pesticide concentration. The experimental results suggested that pH has no significant effect on the adsorption performance of pesticides in water, which may be related to the existing forms of the three pesticides at different pH values (Figs. S1 and S2). The pKa of Met was 13.27, which mainly existed as a neutral molecule in the aqueous media. This means that Met is easy to be protonated at lower pH due to the two protonatable nitrogen atoms contained in Met structure. It can also be concluded that the solubility should be better under acidic conditions, which will lead to the faster release

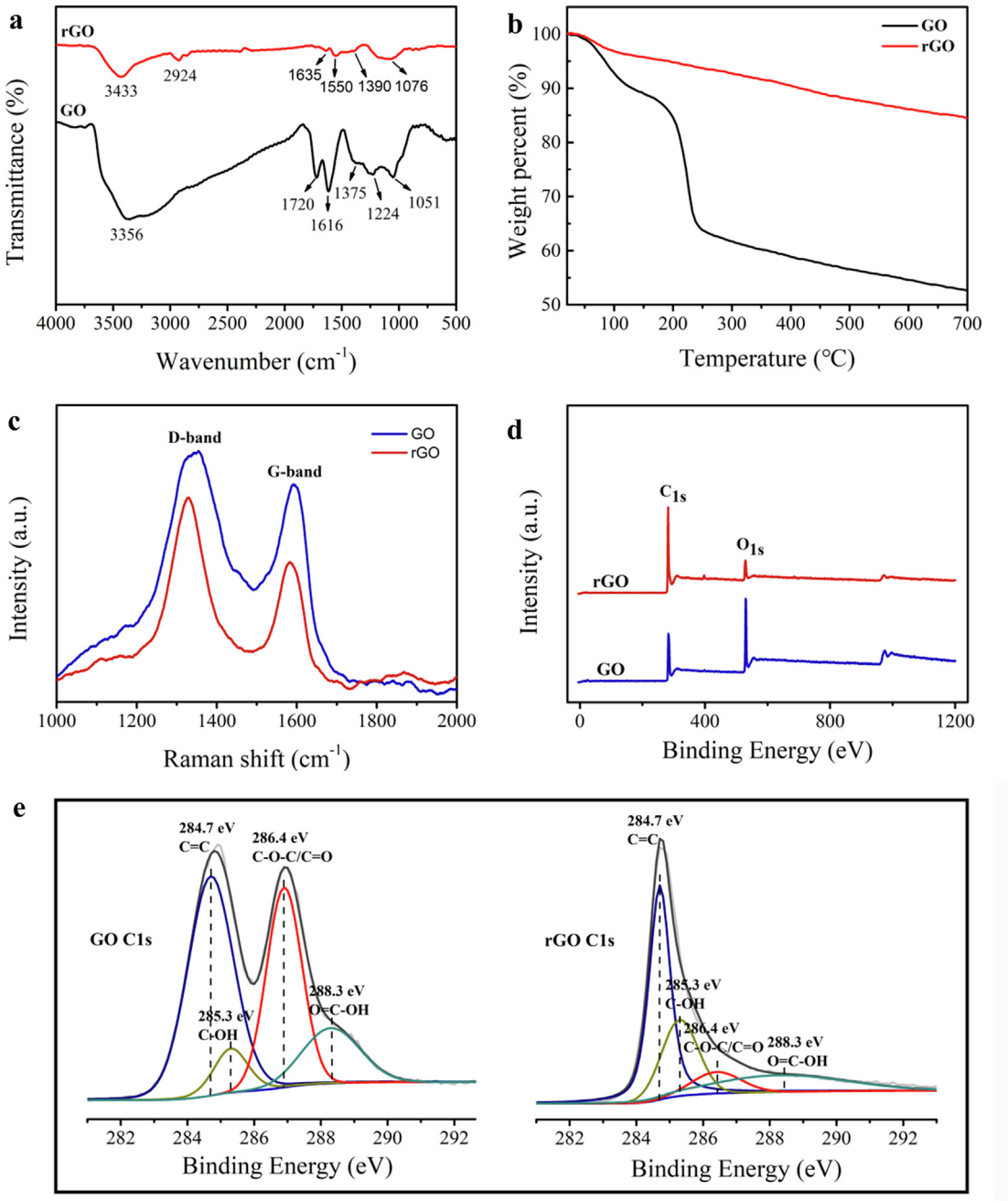

Fig. 2. Characterization of GO and rGO. FT-IR spectra (a); Raman spectra (b); TGA curves (c); wide survey XPS spectra (d) and C1s core level scan spectra resolved results (e).

of Met from GO and rGO and thereby decrease the adsorption capacity of graphene-materials for Met. However, graphene-materials are negatively charged over the whole pH range, which can be ascribed to the ionization of carboxylic acid groups. Thus, there might be electrostatic attraction between graphene-materials and pesticides, which could improve the adsorption capacity of GO and rGO for the protonated Met molecules. Comprehensively, these two factors may offset each other, making pH have little effect on the adsorption efficiency of Met by GO and rGO. In addition, the values of pKa for Ace and Azo were −0.44 and −0.93, respectively, indicating that they exist in the form of anions. Their charges are not affected by the variation of solution pH. Therefore, the adsorption capacities of Ace and Azo by GO and rGO are not affected by changes in pH. Therefore, pH 7 was chosen as the appropriate experimental condition. The results revealed that the maximum adsorption efficiency of adsorbent occurred at 1 mg, and no significant increase in adsorption efficiency was observed above 1 mg. With increasing pesticide concentration, the adsorption capacity gradually increased and finally reached saturation.

3.3. Adsorption kinetics

Fig. 4 shows the changes in adsorption amount (Q_t) of three pesticides by GO and rGO with adsorption time. The adsorption capacity of GO and rGO for Met, Ace and Azo increased rapidly in the first half hour, and then showed a decrease at 3 h and stayed stable thereafter. Hence, the reaction time of 9 h was selected as the equilibrium time for the following experiments. In addition, GO and rGO exhibited different adsorption capacities for the three

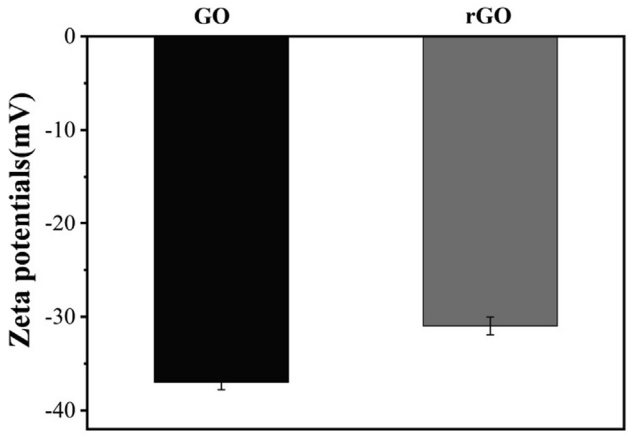

Fig. 3. Zeta potential analysis for GO and rGO.

pesticides, which may be ascribed to the different structure of pesticides (Fig. 4).

Adsorption kinetics is usually employed to describe the adsorption rate of the solute by the adsorbent and the adsorption type. Here, the pseudo first-order, pseudo second-order and Elovich models (Eqs. (2), (3) and (4), respectively) were used to describe most adsorption reactions. Table 2 lists the corresponding fitting parameters and determination coefficients (R^2). In this work, both the pseudo second-order and the Elovich kinetic models could better fit the data than the pseudo first-order model, providing R^2 values >0.998. These results indicate that the adsorption of the three pesticides by GO and rGO may be controlled by multiple mechanisms.

3.4. Adsorption isotherms

Equilibrium adsorption isotherms are useful for investigating the interaction between solute and adsorbent, which is important for the design of adsorption systems. The experimental data of adsorption isotherms were fitted with the Langmuir, Freundlich, Temkin, Dubinin–Radushkevich and Sips models, and the corresponding fitting parameters are shown in Fig. 5 and Table S5. The Sips isotherm model had the best fitting for the experimental data, which could better describe the adsorption process of the three pesticides on both GO and rGO. The Sips model exponent (b_s) is related to the heterogeneity of the adsorption process. All Met, Ace and Azo had b_s values above 1, demonstrating that the adsorption was a heterogeneous process [49,50]. The Sips model can describe the adsorption occurring on an adsorbent with a heterogeneous surface structure [51]. GO and rGO have various functional groups such as hydroxyl groups, which may account for the heterogeneous adsorption process of the pesticides. And these various functional groups can also explain why the sips model had the best fitting.

3.5. Adsorption thermodynamics

To investigate the effect of temperature on the adsorption performance and mechanism, a thermodynamic study was carried out by varying the temperature from 298 to 318 K. The calculated results of the thermodynamic parameters are shown in Table 3. The negative value of ΔH suggested that the adsorption was an exothermic process. These results indicate that high temperature is not conducive to the adsorption of the three pesticides onto GO and rGO. The negative ΔS values reflected decreasing randomness at the solid/liquid interface during the adsorption process. A negative ΔG value was obtained, indicating that the adsorption was a spontaneous process [52]. With the increase of temperature, the ΔG value decreased, indicating that the adsorption efficiency is better at low temperature. The value of ΔG within the range between −80 and −400 kJ/mol indicates a chemisorption process, while the variation between 0 and −20 kJ/mol is typical for physisorption. In the present work, the ΔG values ranged from −1 to −5 kJ/mol, demonstrating that the adsorption of three pesticides by GO and rGO is a physisorption process.

3.6. FCCD development

According to the experimental results obtained from FCCD, the statistical relationships among the response and the variables were obtained and the final equations in terms of actual factors were predicted as Eqs. (17) and (S1)–(S5).

$$\begin{aligned}\text{Adsorption Capacity of Met onto GO } (Y_1, q_e) = {} & -39.51829 \\ & + 19.85982X_1 + 0.73108X_2 + 2.40761X_3 - 0.20718X_1X_2 \\ & + 0.031234X_1X_3 - 0.017515X_2X_3 - 3.24335X_1{}^2 \\ & - 0.00291X_2{}^2 - 0.00921X_3{}^2\end{aligned} \tag{17}$$

ANOVA was employed to evaluate for the significance of the variables and model fitting [53]. The acquired results are summarized in Table 4 and Table S6-S10. The higher F-test values and lower P-values (<0.0001) were obtained, indicating that the model is significant. The lack-of-fit value was non-significant, confirming

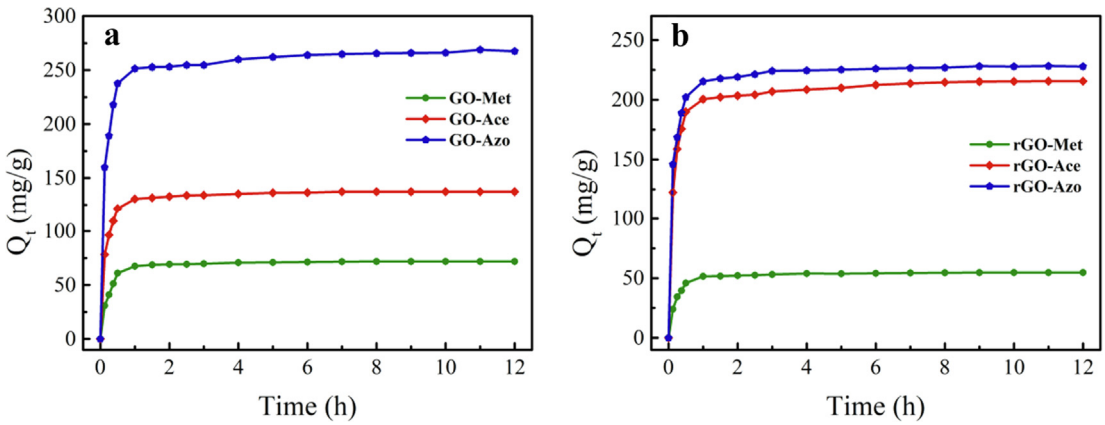

Fig. 4. Effects of adsorption time on the adsorption of pesticides onto GO(a) and rGO (b).

Table 2
Adsorption kinetic models and related parameters.

Materials	Pesticides	Pseudo-first order			Pseudo-second order			Elovich		
		Q_e (mg/g)	K_1 (1/h)	R^2	Q_e (mg/g)	K_2 (g/(mg ·h))	R^2	α (mg/g)	β (g/mg)	R^2
GO	Met	70.31	5.4132	0.9957	71.55	0.2819	0.9989	8.46×10^9	0.3274	0.9979
	Ace	134.89	5.9862	0.9967	136.83	0.1863	0.9991	1.23×10^{12}	0.2039	0.9985
	Azo	259.33	4.8543	0.9952	264.69	0.0621	0.9986	9.02×10^{11}	0. 1025	0.9992
rGO	Met	53.29	6.0397	0.9952	34.11	0.4489	0.9982	1.20×10^{11}	0.4886	0.9984
	Ace	208.51	5.3177	0.9934	212.63	0.0857	0.9977	2.92×10^{10}	0.1111	0.9990
	Azo	223.58	4.5671	0.9969	228.39	0.0665	0.9997	2.14×10^{10}	0.1022	0.9979

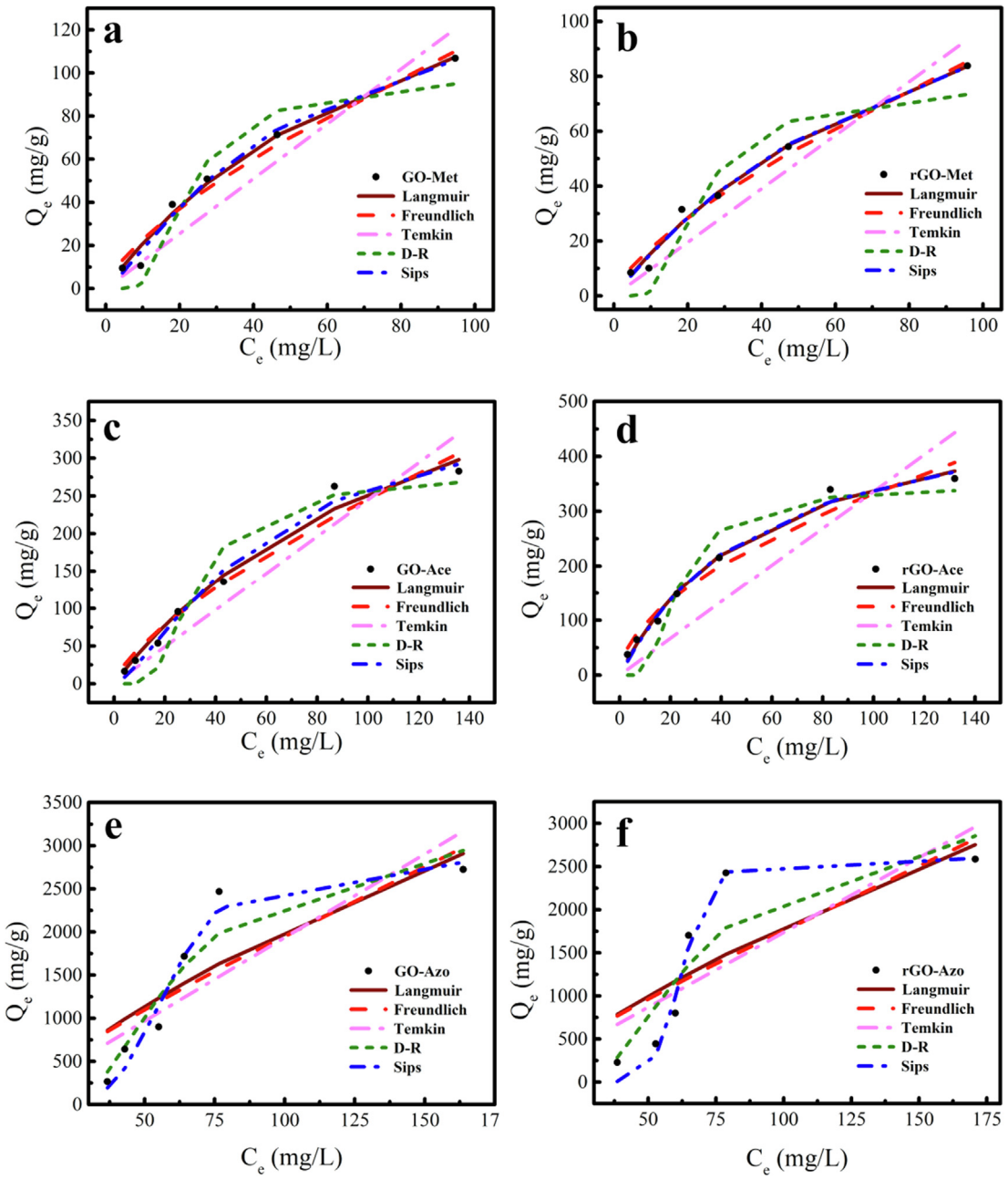

Fig. 5. Adsorption isotherm fitting curves of GO adsorption for Met (a), rGO adsorption for Met (b), GO adsorption for Ace (c), rGO adsorption for Ace (d), GO adsorption for Azo (e), and rGO adsorption for Azo (f).

the adequacy of the developed model. The values of R^2 and Adj R-Squared parameters (Adj.R^2) were very close to 1, indicating that the adsorption of pesticides by GO and rGO can be well described and predicted by the developed model. Coefficient variation (CV) determines the reliability of the performed tests and a supreme degree of precision, and its value of <10% is reproducible [54].

Table 3
Adsorption thermodynamics and related parameters.

Materials	Pesticides	Temperature (K)	ΔG kJ/mol	ΔH kJ/mol	ΔS (kJ/(mol·K))
GO	Met	298	−2.80	−17.27	−0.05
		308	−2.60		
		318	−1.84		
	Ace	298	−2.74	−20.64	−0.06
		308	−2.22		
		318	−1.54		
	Azo	298	−4.91	−44.57	−0.13
		308	−4.08		
		318	−2.27		
rGO	Met	298	−2.39	−8.05	−0.02
		308	−2.25		
		318	−2.01		
	Ace	298	−3.49	−18.96	−0.05
		308	−2.55		
		318	−2.43		
	Azo	298	−4.40	−38.57	−0.11
		308	−3.45		
		318	−2.11		

Table 4
ANOVA for the adsorption capacity of Met onto GO.

Source	Sum of squares	Degree of freedom (df)	Mean squares	F-value	Probability P-value > F
Model	16420.42	9	1824.49	246.07	<0.0001
X_1	138.19	1	138.19	18.64	0.0015
X_2	626.81	1	626.81	84.54	<0.0001
X_3	13913.00	1	13913.00	1876.46	<0.0001
X_1 X_2	57.51	1	57.51	7.76	0.0193
X_1 X_3	26.54	1	26.54	3.58	0.0878
X_2 X_3	498.12	1	498.12	67.18	<0.0001
X_1^2	26.32	1	26.32	3.55	0.0889
X_2^2	0.23	1	0.23	0.031	0.8629
X_3^2	930.28	1	930.28	125.47	<0.0001
Residual	74.14	10	7.41		
Lack of Fit	55.23	5	11.05	2.92	0.1323
Pure Error	18.91	5	3.78		
Cor. Total	16494.56	19			
R^2 = 0.9955	Adj.R^2 = 0.9915	Pred.R^2 = 0.9643	Coefficient Variation (CV %) = 5.21	Adeq. Precision (AP) = 53.808	

The low values of CV, i.e., 5.21% (GO-Met), 9.75 % (rGO-Met), 3.48 % (GO-Ace), 1.41 % (rGO-Ace), 2.61 % (GO-Azo) and 3.03 % (rGO-Azo), indicated the reproducibility of the model. Besides, Adeq. precision (AP) higher than 4 confirmed the appropriate relationship between the experimental and predicted results [55].

3.7. Effects of different factors on responses and optimization

The plots of three-dimensional surface response are graphical representations of the regression equation, which is a function of two factors while holding all other factors at fixed levels. The plots can help to understand the main effects and interaction effects of two factors. Fig. 6 demonstrates that the adsorption capacity of three pesticides onto GO and rGO increased with increasing initial pesticide concentration. On the contrary, the adsorption capacity of pesticides decreased with increasing temperature, which may be due to the exothermic adsorption process. Moreover, the results revealed that the adsorption capacity is enhanced by an increase of the contact time (Figs. S3–S4).

The optimal conditions of adsorption time, temperature and initial concentration of three pesticides onto GO and rGO are presented in Table S11. The predicted adsorption capacity of GO for Met, Ace and Azo was 105.23, 286.45 and 2730.51 mg/g; while that of rGO was 92.61, 357.37 and 2682.04 mg/g, respectively. Desirability factor is another important parameter to evaluate the best adsorption conditions. In this work, the desirability for all the optimal conditions was very close to 1, indicating that adsorption conditions can obtain the highest adsorption capacity for Met, Ace and Azo onto GO and rGO.

To validate the reliability of FCCD optimization, four experiments (n = 4) were conducted under the optimal conditions, and the adsorption capacities of three pesticides by GO and rGO were obtained and shown in Table S11. The predicted values were very similar to the experimental results, suggesting that the models can accurately describe the relationship between the independent parameters and response.

3.8. Characterization of adsorbents loaded with pesticides.

The SEM images of GO and rGO before and after adsorption of the three pesticides are shown in Fig. 7. Fig. 7a shows that GO consists of folded and wrinkled sheets randomly aggregated in a disordered structure, and rGO showed flaky structure and scale-like layered structure overlapped to form a compact structure (Fig. 7e). Fig. S5 shows the SEM images for the initial structures of Met, Ace and Azo. Flake-, needle- and block-like structures could be observed for Met, Ace and Azo, respectively. In addition, after the adsorption of three pesticides, it could be clearly seen that the surfaces of the three pesticides were completely covered by GO dispersion (Fig. 7b–d) or rGO dispersion (Fig. 7f–h). Moreover,

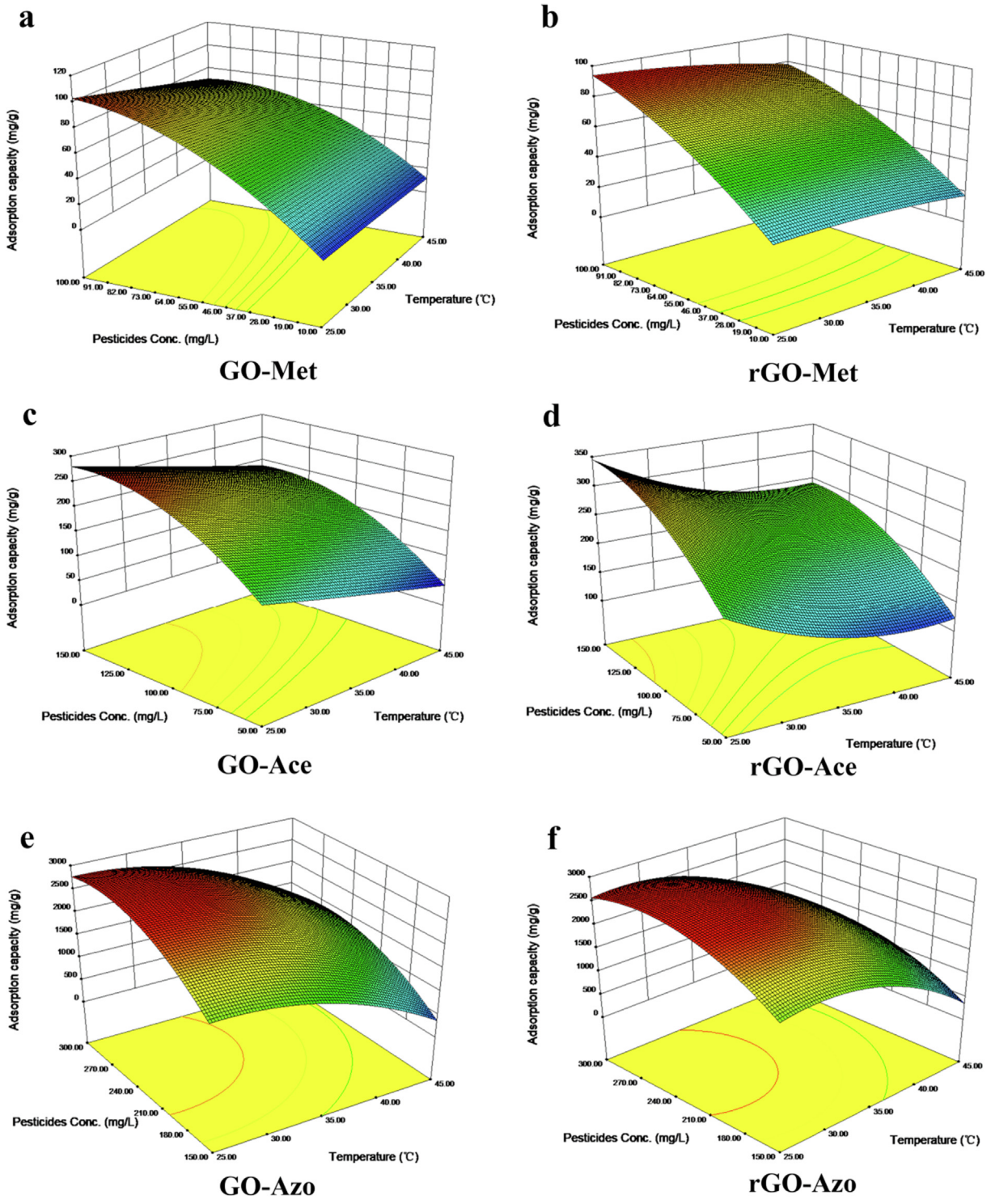

Fig. 6. Three-dimensional surface plots of the effect of pesticides concentration and temperature on adsorption capacity of GO and rGO.

the element species and distribution are shown in Fig. S6. The structural elements of GO and rGO were mainly C and O, and there was a small amount of S, while no N was found [56]. The structural elements of Met included C, H, N and S. The existence of N in Fig. S6 (a) and (d) demonstrated the adsorption of Met on GO and rGO. The structural elements of Ace and Azo comprised C, O and N (Fig. S6b,c, e,f), and elemental analysis confirmed that Ace and Azo were adsorbed on GO and rGO.

The FT-IR spectra of Met, GO and GO after Met adsorption (GO-Met) are shown in Fig. 8a. For Met, the peak at 3300 cm^{-1} can be attributed to the N—H flexural vibration. The N—H bending and C—N stretching vibrations are in the 1400–1700 cm^{-1} region [57,58]. The characteristic absorption peaks at 1720 and 1247 cm^{-1} are due to C=O and C—O stretching vibrations, and those at 2924 and 2890 cm^{-1} are attributed to C—H stretching vibration [27,59]. After adsorption of the pesticides onto GO, there

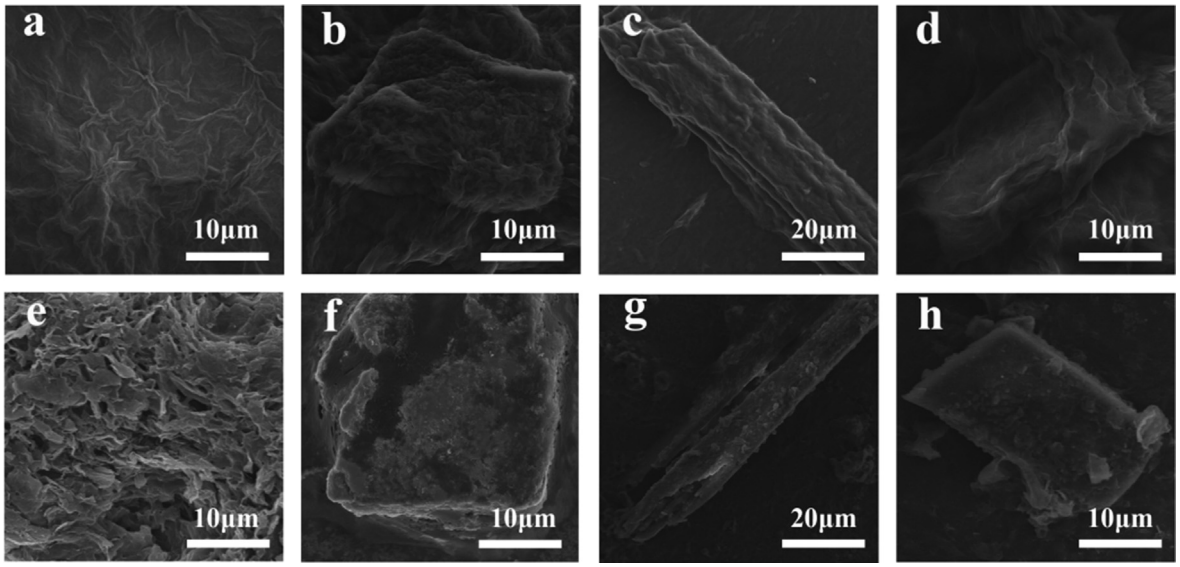

Fig. 7. SEM images of GO (a), GO after Met (b), Ace (c), and Azo adsorption (d), rGO (e), rGO after Met (f), Ace (g), and Azo adsorption (h).

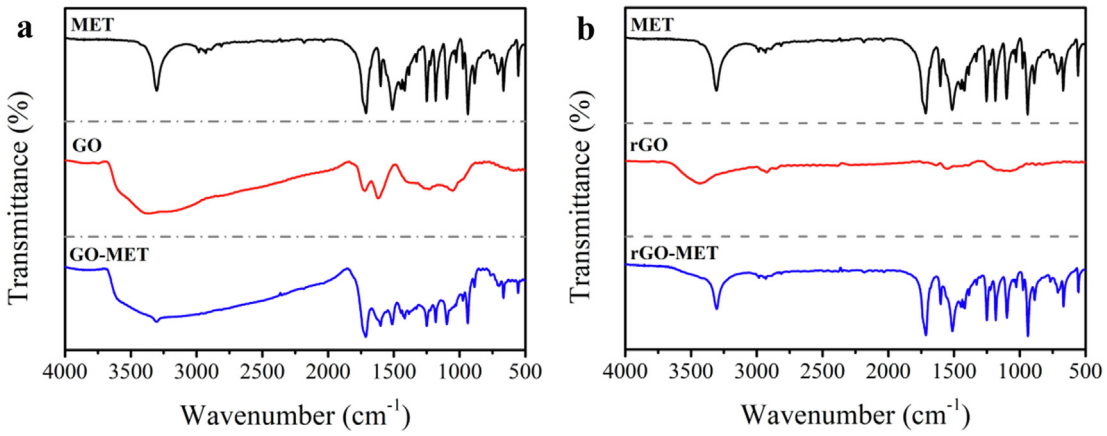

Fig. 8. FT-IR spectra of GO (a) and rGO (b) before and after the adsorption of Met.

was an obvious shift as well as a decrease in the intensity of the peaks corresponding to N-H, C—H and C—N stretching and bending frequency. None of these new peaks was observed to appear after pesticide adsorption, indicating that no new covalent bond was formed during the adsorption process. Met adsorption on rGO showed no difference from that on GO (Fig. 8b). The same results were obtained for all the pesticides (Fig. S7). As discussed above, the adsorption of pesticides on GO and rGO is probably a physisorption process.

3.9. Adsorption mechanism

The mechanism for the different adsorption capacities of the three pesticides onto GO/rGO remains unclear. It has been found that the adsorption of GO for pollutants mainly depends on oxygen-containing functional groups and sp^2 carbon π-π conjugated structure in its structure, for which the interaction mechanisms possibly include electrostatic interaction, H-bonding and π-π conjugation in general [60]. We speculate that the different structures of the three pesticides (no aromatic ring, one aromatic ring and three aromatic rings) may contribute to their different adsorption capacities onto GO/rGO. The first possible mechanism is that the π-π conjugation interaction between the aromatic rings in pesticides and graphene-materials facilitates the adsorption of GO and rGO for the pesticide. Increasing aromatic rings in the pesticide structure would lead to stronger π-π conjugation interactions between pesticides and graphene-materials, which would accordingly enhance the adsorption capacity of GO or rGO for the pesticide. This mechanism may explain our result that the adsorption capacities of GO and rGO at equilibrium for the pesticides followed the order of Azo > Ace > Met (Fig. 5). Besides, the large amount of functional groups on GO and rGO, such as –OH and –COOH, could form H-bonding and electrostatic interaction with pesticide molecules, affecting the adsorption capacity of GO or rGO for the pesticide. Compared with rGO, GO had more oxygen-containing groups, which contributed to more H-bonding interactions and electrostatic interactions between GO and pesticides. Therefore, there are significant differences in adsorption capacity for pesticides between GO and rGO. The last possible mechanism may be ascribed to the H-bonding and π-π conjugation between pesticides, which may result in cooperative adsorption. In addition, the π-π conjugation interaction between pesticide molecules is an important adsorption force. More aromatic rings generally represent stronger π-π conjugation interaction between pesticide molecules, which lead to a higher adsorption capacity. Thus, the adsorption capacity of Azo on GO and rGO is much greater than

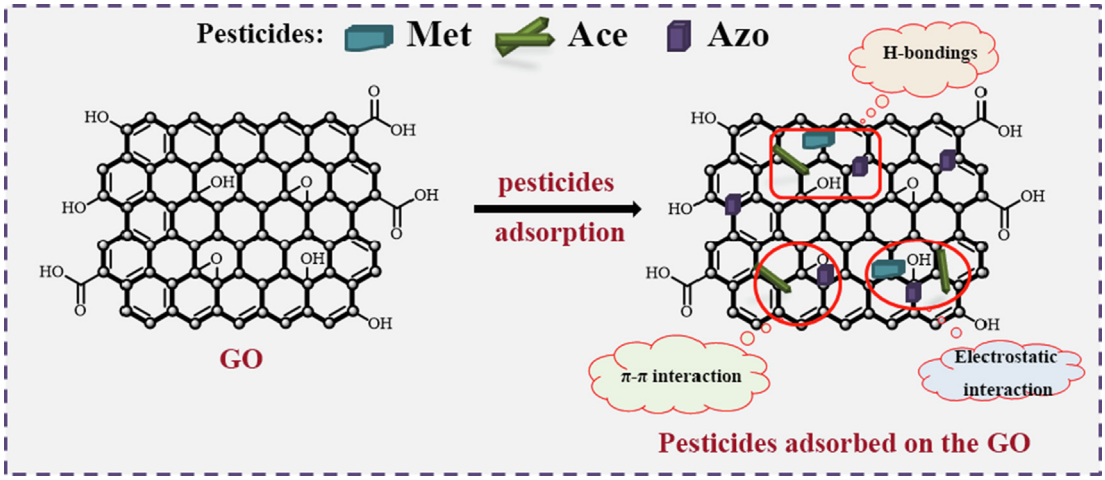

Fig. 9. Possible mechanism for the adsorption of pesticide molecules on GO/rGO.

Table 5
Comparison of adsorption capacities of various adsorbents for pesticide removal.

Pesticide	Adsorbent	Analysis method	Adsorption Capacity	Reference
Met	AS/NZVI/GO	HPLC	59.13 mg g^{-1}	[61]
Met	orange bagasse	HPLC	10.776 mg g^{-1}	[62]
Met	biochar (BC)	UV–Vis	32.42 mg g^{-1}	[63]
Met	GO	HPLC	105.23 mg g^{-1}	This work
Met	rGO	HPLC	92.61 mg g^{-1}	This work
Ace	Biochar (BC)	UV–Vis	4.87 mg g^{-1}	[63]
Ace	Molecularly imprinted polymers (MIP)	HPLC-MS-MS	25.62 mg g^{-1}	[59]
Ace	FeCl3-pistachio shells (MAC)	HPLC	86.10 mg g^{-1}	[64]
Ace	GO	HPLC	286.45 mg g^{-1}	This work
Ace	rGO	HPLC	357.37 mg g^{-1}	This work
Azo	polystyrene (PS)	UPLC-MSMS	20.88 mg g^{-1}	[65]
Azo	polyethylene (PE)	UPLC-MSMS	16.69 mg g^{-1}	[65]
Azo	RS + P(soil:rice straw: peat)	HPLC	78.14 mg g^{-1}	[66]
Azo	GO	HPLC	2730.51 mg g^{-1}	This work
Azo	rGO	HPLC	2682.04 mg g^{-1}	This work

that of other two pesticides. The possible adsorption mechanisms for pesticide molecules on GO and rGO are depicted in Fig. 9.

3.10. Comparison with previous studies

The comparison with other adsorbents used for removal or adsorb pesticides is summarized in Table 5. Compared with other adsorbents, GO and rGO exhibit considerable potential advantages. On the one hand, GO and rGO exhibited high adsorption capacities when used to adsorb three pesticides simultaneously. On the other hand, GO and rGO have a wide range of applications and can be used to remove organic pollutants containing aromatic rings in aqueous solutions. These characteristics make GO and rGO efficient adsorbents that may be widely used.

4. Conclusions

This study investigated the adsorption properties of GO and rGO for Met, Ace and Azo in aqueous solutions. The adsorption experiments demonstrated different adsorption capacities of GO and rGO for the three pesticides. The pseudo second-order and Elovich kinetic models could well fit the experimental data, providing R^2 values > 0.998. Adsorption isotherm analysis revealed that the Sips model could best fit the adsorption process of the three pesticides on both GO and rGO, indicating that the adsorption is a heterogeneous process. Besides, the thermodynamic study indicated that the adsorption process is exothermic and physical adsorption. The effects of the main operating parameters on pesticides removal from aqueous solutions using GO and rGO were investigated and optimized via RSM. The maximum adsorption capacity of GO for Met, Ace and Azo was 105.23, 286.45 and 2730.51 mg/g; while that of rGO was 92.61, 357.37 and 2682.04 mg/g, respectively. Increasing aromatic rings in the pesticide structure would lead to stronger π-π conjugation interaction between pesticides and graphene-materials, which would accordingly enhance the adsorption capacity of GO or rGO for the pesticide. In addition, the H-bonding and electrostatic interaction between pesticide molecules and adsorbents also plays a synergistic role in promoting the adsorption. This work provides new insights into the application of GO and rGO as green adsorbents for removal of pesticides and other organic pollutants containing aromatic rings from water.

Data availability

The data that has been used is confidential.

Declaration of Competing Interest

The authors declare that they have no known competing financial interests or personal relationships that could have appeared to influence the work reported in this paper.

Acknowledgements

This research was funded by National Natural Science Foundation of China (31501680), Key Research and Development Program of Hebei Province (21326507D), Modern Agricultural Industrial Technology System Innovation Team of Hebei Province (coarse grains and beans, HBCT2018070404), Science and Technology Research Project for Colleges and Universities in Hebei Province (BJ2020049), Postgraduate Innovation Funding Project of Hebei Normal University of Science and Technology (CXZZ202103).

Appendix A. Supplementary material

Supplementary data to this article can be found online at https://doi.org/10.1016/j.molliq.2022.119967.

References

[1] K. Kapinder, A.K. Dangi Verma, Efficient & eco-friendly smart nano-pesticides: emerging prospects for agriculture, Mater. Today: Proc. 45 (2021) 3819–3824, https://doi.org/10.1016/j.matpr.2021.03.211.
[2] M. Zhao, P. Li, H. Zhou, L. Hao, H. Chen, X. Zhou, pH/redox dual responsive from natural polymer-based nanoparticles for on-demand delivery of pesticides, Chem. Eng. J. 435 (2022) 134861, https://doi.org/10.1016/j.cej.2022.134861.
[3] P. Vikesland, E. Garner, S. Gupta, S. Kang, A. Maile-Moskowitz, N. Zhu, Differential Drivers of Antimicrobial Resistance across the World, Acc. Chem. Res. 52 (2019) 916–924. <https://doi.org/ 10.1021/acs.accounts.8b00643>.
[4] D.O. Ferraro, R.D. Paula, A fuzzy knowledge-based model for assessing risk of pesticides into the air in cropping systems, Sci. Total Environ. 820 (2022) 153158, https://doi.org/10.1016/j.scitotenv.2022.153158.
[5] S. Popli, P.C. Badgujar, T. Agarwal, B. Bhushan, V. Mishra, Persistent organic pollutants in foods, their interplay with gut microbiota and resultant toxicity, Sci. Total Environ. 832 (2022) 155084, https://doi.org/10.1016/j.scitotenv.2022.155084.
[6] L.A. Thompson, W.S. Darwish, Environmental chemical contaminants in food: review of a global problem, J. Toxicol. 2019 (2019) 2345283, https://doi.org/10.1155/2019/2345283.
[7] L. Mamy, K. Bonnot, P. Benoit, C. Bockstaller, E. Latrille, V. Rossard, R. Servien, D. Patureau, L. Prevost, F. Pierlot, C. Bedos, Assessment of pesticide volatilization potentials to atmosphere from their molecular properties using the TyPol tool, J. Hazard. Mater. 415 (2021) 125613, https://doi.org/10.1016/j.jhazmat.2021.125613.
[8] Y. Yang, S. Hao, X. Lei, J. Chen, G. Fang, J. Liu, S. Wang, X. He, Design of metalloenzyme mimics based on self-assembled peptides for organophosphorus pesticides detection, J. Hazard. Mater. 428 (2022) 128262, https://doi.org/10.1016/j.jhazmat.2022.128262.
[9] B. Lellis, C. Fávaro-Polonio, J.A. Pamphile, J.C. Polonio, Effects of textile dyes on health and the environment and bioremediation potential of living organisms, Biotechnol. Res. Innov. 3 (2019) 275–290, https://doi.org/10.1016/j.biori.2019.09.001.
[10] Z. Wang, W. Ouyang, M. Tysklind, C. Lin, B. Wang, Seasonal variations in atrazine degradation in a typical semienclosed bay of the Northwest Pacific Ocean, Environ. Pollut. 283 (2021) 117072, https://doi.org/10.1016/j.envpol.2021.117072.
[11] H. Karimi, S. Mahdavi, B.A. Lajayer, E. Moghiseh, T. Astatkie, Insights on the bioremediation technologies for pesticide contaminated soils, Environ. Geochem. Heal. (2021), https://doi.org/10.1007/s10653-021-01081-z.
[12] V. Góngora-Echeverría, R. García-Escalante, R. Rojas-Herrera, G. Giácoman-Vallejos, C. Ponce-Caballero, Pesticide bioremediation in liquid media using a microbial consortium and bacteria-pure strains isolated from a biomixture used in agricultural areas, Ecotox. Environ. Safe 200 (2020) 110734, https://doi.org/10.1016/j.ecoenv.2020.110734.
[13] T. Pham, H. Bui, T. Bui, Advanced oxidation processes for the removal of pesticides – ScienceDirect, Curr. Dev. Biotechnol. Bioeng. (2020) 309–330, https://doi.org/10.1016/B978-0-12-819594-9.00013-9.
[14] J. Kodali, S. Pavuluri, B. Arunraj, A.S.K. Kumar, N. Rajesh, Tapping the potential of a glucosamine polysaccharide-diatomaceous earth hybrid adsorbent in the solid phase extraction of a persistent organic pollutant and toxic pesticide 4,4′-DDT from water, RSC Adv. 12 (2022) 5489–5500, https://doi.org/10.1039/d1ra07868b.
[15] S.D. Khairnar, A.N. Kulkarni, S.G. Shinde, S.D. Marathe, V.S. Shrivastava, Synthesis and characterization of 2-D La-doped Bi_2O_3 for photocatalytic degradation of Organic Dye and Pesticide, J. Photoch. Photobio. A. 6 (2021) 100030, https://doi.org/10.1016/j.jpap.2021.100030.
[16] F. Soltani-Nezhad, A. Saljooqi, A. Mostafavi, T. Shamspur, Synthesis of Fe_3O_4/CdS-ZnS nanostructure and its application for photocatalytic degradation of chlorpyrifos pesticide and brilliant green dye from aqueous solutions, Ecotox. Environ. Safe. 189 (2020) 109886, https://doi.org/10.1016/j.ecoenv.2019.109886.
[17] Y. Wang, C. Lin, X. Liu, W. Ren, X. Huang, M. He, W. Ouyang, Efficient removal of acetochlor pesticide from water using magnetic activated carbon: Adsorption performance, mechanism, and regeneration exploration, Sci. Total Environ. 778 (2021) 146353, https://doi.org/10.1016/j.scitotenv.2021.146353.
[18] M.H. Dehghani, S. Kamalian, M. Shayeghi, M. Yousefi, Z. Heidarinejad, S. Agarwal, V.K. Gupta, High-performance removal of diazinon pesticide from water using multi-walled carbon nanotubes - ScienceDirect, Microchem. J. 145 (2019) 486–491, https://doi.org/10.1016/j.microc.2018.10.053.
[19] P. Wang, X. Liu, B. Yu, X. Wu, J. Xu, F. Dong, Y. Zheng, Characterization of peanut-shell biochar and the mechanisms underlying its sorption for atrazine and nicosulfuron in aqueous solution, Sci. Total Environ. 702 (2020) 134767, https://doi.org/10.1016/j.scitotenv.2019.134767.
[20] K. An, H. Kang, D. Tian, Fabrication and evaluation of controllable core/shell magnetic molecular imprinted polymers based on konjac glucomannan for trichlorfon, J. Appl. Polym. Sci. 137 (2020), https://doi.org/10.1002/APP.48910.
[21] Z. Liu, Q. Wang, X. Huang, X. Qian, Surface functionalization of graphene oxide with hyperbranched polyamide-amine and microcrystalline cellulose for efficient adsorption of heavy metal ions, ACS Omega 7 (2022) 10944–10954, https://doi.org/10.1021/acsomega.1c06647.
[22] X. Zhao, Z. Wu, Z. Zhang, N. Wang, C. Tao, J. Wang, H. Gong, The polymer composite electrolyte with polyethylene oxide-grafted graphene oxide as fillers toward stable highcurrent density lithium metal anodes, Mater. Res. Exp.105305 8 (2021), https://doi.org/10.1088/2053-1591/ac0b0a.
[23] H.R. Nodeh, A. Kamboh, W. Ibrahim, B.H. Jume, H. Sereshti, M.M. Sanagi, Equilibrium, kinetic and thermodynamic study of pesticides removal from water using novel glucamine-calix [4] arene functionalized magnetic graphene oxide, Environ. Sci.: Process. Impacts 21 (2019) 714–726, https://doi.org/10.1039/C8EM00530C.
[24] Z. Dehghani, M. Sedghi-Asl, M. Ghaedi, M.M. Sabzehmeidani, E. Adhami, Ultrasound-assisted adsorption of paraquat herbicide from aqueous solution by graphene oxide/ mesoporous silica, J. Environ. Chem. Eng.105043 9 (2021), https://doi.org/10.1016/j.jece.2021.105043.
[25] X. Wang, H. Xie, Z. Wang, K. He, D. Jing, Graphene oxide as a multifunctional synergist of insecticides against lepidopteran insect, Environ. Sci.: Nano 6 (2018) 75–84, https://doi.org/10.1039/c8en00902c.
[26] P. Ren, D. Yan, X. Ji, T. Chen, Z. Li, Temperature dependence of graphene oxide reduced by hydrazine hydrate, Nanotechnology055705 22 (2010), https://doi.org/10.1088/0957-4484/22/5/055705.
[27] H. Li, F. Wang, J. Li, S. Deng, S. Zhang, Adsorption of three pesticides on polyethylene microplastics in aqueous solutions: Kinetics, isotherms, thermodynamics, and molecular dynamics simulation, Chemosphere128556 264 (2021), https://doi.org/10.1016/j.chemosphere.2020.128556.
[28] B. Gao, A. Zimmerman, M. Zhang, C. Hao, Synthesis, characterization, and dye sorption ability of carbon nanotube–biochar nanocomposites, Chem. Eng. J. 236 (2014) 39–46, https://doi.org/10.1016/j.cej.2013.09.074.
[29] H. Kesarwani, A. Saxena, A. Mandal, S. Sharma, Anionic/nonionic surfactant mixture for enhanced oil recovery through the investigation of adsorption, interfacial, rheological, and rock wetting characteristics, Energ Fuel. 35 (2021) 3065–3078, https://doi.org/10.1021/acs.energyfuels.0c03767.
[30] F. Banisheykholeslami, M. Hosseini, G.N. Darzi, Design of PAMAM grafted chitosan dendrimers biosorbent for removal of anionic dyes: adsorption isotherms, kinetics and thermodynamics studies, Int. J. Biol. Macromol. 177 (2021) 306–316, https://doi.org/10.1016/j.ijbiomac.2021.02.118.
[31] V. Ashouri, K. Adib, M.R. Nasrabadi, A new strategy for the adsorption and removal of fenitrothion from real samples by active-extruded MOF (AE-MOF UiO-66) as an adsorbent, New J. Chem. 45 (2021) 5029–5039, https://doi.org/10.1039/d0nj05693f.
[32] M.H. To, P. Hadi, C. Hui, C.S.K. Lin, G. Mckay, Mechanistic study of atenolol, acebutolol and carbamazepine adsorption on waste biomass derived activated carbon, J. Mol. Liq. 241 (2017) 386–398, https://doi.org/10.1016/j.molliq.2017.05.037.
[33] N.T. Hai, S.J. You, A. Hosseini-Bandegharaei, H.P. Chao, Mistakes and inconsistencies regarding adsorption of contaminants from aqueous solutions: a critical review, Water Res. 120 (2017) 88–116, https://doi.org/10.1016/j.watres.2017.04.014.
[34] V.W.O. Wanjeri, C.J. Sheppard, A.R.E. Prinsloo, J.C. Ngila, P.G. Ndungu, Isotherm and kinetic investigations on the adsorption of organophosphorus pesticides on graphene oxide based silica coated magnetic nanoparticles functionalized with 2-phenylethylamine, J. Environ. Chem. Eng. 6 (2018) 1333–1346, https://doi.org/10.1016/j.jece.2018.01.064.
[35] Z. Liu, F. Zhang, Removal of lead from water using biochars prepared from hydrothermal liquefaction of biomass, J. Hazard. Mater. 167 (2009) 933–939, https://doi.org/10.1016/j.jhazmat.2009.01.085.
[36] F. Taktak, Z. İlbay, S. Şahin, Evaluation of 2, 4-D removal via activated carbon from pomegranate husk/polymer composite hydrogel: optimization of process parameters through face centered composite design, Korean J. Chem. Eng. 32 (2015) 1–10, https://doi.org/10.1007/s11814-015-0010-5.
[37] Z. İlbay, A. Haşimoğlu, O.K. Özdemir, F. Gedik, S. Şahin, Highly efficient recovery of biophenols onto graphene oxide nanosheets: Valorisation of a biomass, J. Mol. Liq. 246 (2017) 208–214, https://doi.org/10.1016/j.molliq.2017.09.046.
[38] D. Surabhi, J. Sah, P. Shabir, S. Gupta, Mozumdar, imidazole-functionalized porous graphene oxide nanosheets loaded with palladium nanoparticles for the oxidative amidation of aldehydes, ACS Appl. Nano Mater. 5 (2022) 5776–5792, https://doi.org/10.1021/acsanm.2c00859.

[39] Y. Tian, Z. Bi, G. Cui, Study on the corrosion resistance of graphene oxide-based epoxy zinc-rich coatings, Polymers 13 (2021) 1657, https://doi.org/10.3390/polym13101657.
[40] S. Sharma, B. Singh, P. Bindra, P. Panneerselvam, V. Shanmugam, Triple-smart eco-friendly chili anthracnose control agro-nanocarrier, ACS Appl. Mater. Inter. 13 (2021) 9143–9155, https://doi.org/10.1021/acsami.0c18797.
[41] C. Zhao, P. Hong, Y. Li, X. Song, Y. Yang, Mechanism of adsorption of tetracycline–Cu multiollutants by graphene oxide (GO) and reduced graphene oxide (rGO), J. Chem. Technol. Biot. 94 (2018), https://doi.org/10.1002/jctb.5864.
[42] Y. Xie, W. Liu, L. Liang, C. Liu, F. Zhang, Incorporation of silica network and modified graphene oxide into epoxy resin for improving thermal and anticorrosion properties, J. Appl. Polym. Sci. 137 (2020) 49405, https://doi.org/10.1002/app.49405.
[43] S. Manavalan, J. Ganesamurthi, S.M. Chen, P. Veerakumar, K. Murugan, A robust Mn@FeNi-S/graphene oxide nanocomposite as a high efficiency catalyst for the non-enzymatic electrochemical detection of hydrogen peroxide, Nanoscale 12 (2020), https://doi.org/10.1039/C9NR09148C.
[44] M. Velásquez-Rojas, F.F. Contreras-Torres, V. Meza-Laguna, E. Alvarez-Zauco, E. V. Basiuk, Solvent-free functionalization of graphene oxide powder and paper with aminobenzo-crown ethers and complexation with alkali metal cations, Mater. Chem. Phys. 260 (2021) 124127, https://doi.org/10.1016/j.matchemphys.2020.124127.
[45] W.M.E.M.M. Daniyal, Y.W. Fen, S. Saleviter, N. Chanlek, H. Nakajima, J. Abdullah, N.A. Yusof, X-Ray Photoelectron Spectroscopy Analysis of Chitosan–Graphene Oxide-Based Composite Thin Films for Potential Optical Sensing Applications, Polymers 13 (2021) 478. <https://doi.org/10.3390/polym13030478>.
[46] H. Yu, B. Wang, S. Zhou, M. Zhu, W. Feng, Polyvinylpyrrolidone functionalization induces deformable structure of graphene oxide nanosheets for lung-targeting delivery, Nano Today 38 (2021) 101151, https://doi.org/10.1016/j.nantod.2021.101151.
[47] H. Kim, S.O. Kang, S. Park, H.S. Park, Adsorption isotherms and kinetics of cationic and anionic dyes on three-dimensional reduced graphene oxide macrostructure, J. Ind. Eng. Chem. 21 (2015) 1191–1196, https://doi.org/10.1016/j.jiec.2014.05.033.
[48] K. Amini, S.S. Amiri, A. Ghasemi, S. Mirvalad, A.H. Korayem, Evaluation of the dispersion of metakaolin– graphene oxide hybrid in water and cement pore solution: can metakaolin really improve the dispersion of graphene oxide in the calcium-rich environment of hydrating cement matrix?, RSC Adv 11 (2021) 18623–18636, https://doi.org/10.1039/d1ra01504d.
[49] S. álvarez, R.S. Ribeiro, H.T. Gomes, J.L. Sotelo, J. García, Synthesis of carbon xerogels and their application in adsorption studies of caffeine and diclofenac as emerging contaminants, Chem. Eng. Res. Des. 95 (2015) 229–238. <http://dx.doi.org/10.1016/j.cherd.2014.11.001>.
[50] J. Fan, X. Ran, Y. Ren, C. Wang, J. Yang, W. Teng, L. Zou, Y. Sun, B. Lu, Y. Deng, Ordered mesoporous carbonaceous materials with tunable surface property for enrichment of hexachlorobenzene, Langmuir 32 (2016) 9922–9929, https://doi.org/10.1021/acs.langmuir.6b02258.
[51] M.H. Dehghani, M. Mohammadi, M.A. Mohammadi, A.H. Mahvi, K. Yetilmezsoy, A. Bhatnagar, B. Heibati, G. Mckay, Equilibrium and kinetic studies of trihalomethanes adsorption onto multi-walled carbon nanotubes, Water Air Soil Pollut. 227 (2016) 332, https://doi.org/10.1007/s11270-016-3029-2.
[52] K. Momina, Ahmad, Remediation of anionic dye from aqueous solution through adsorption on polyaniline/FO nanocomposite-modelling by artificial neural network (ANN), J. Mol. Liq. 360 (2022) 119497, https://doi.org/10.1016/j.molliq.2022.119497.
[53] S. Yadav, A. Yadav, N. Bagotia, N. Sharma, A.K. Sharma, S. Kumar, Simultaneous adsorption of three anionic dyes at neutral pH from their individual and multi-component systems on a CTAB modified Pennisetum glaucum based carbon nanotube green composite: adsorption mechanism and process optimization by Box-Behnken design model, J. Mol. Liq. 358 (2022) 119223, https://doi.org/10.1016/j.molliq.2022.119223.
[54] V. Kumar, P. Saharan, A.K. Sharma, I. Kaushal, S. Dhuan, Silver embellished PANI/CNT nanocomposite for antimicrobial activity and sequestration of dye based on RSM modeling, Environ. Technol. 41 (2020) 2991–3003, https://doi.org/10.1080/09593330.2019.1593512.
[55] S. Bagheri, M. Ghaedi, A. Asfaram, E.A. Dil, H. Javadian, RSM-CCD design of malachite green adsorption onto activated carbon with multimodal pore size distribution prepared from Amygdalus scoparia: kinetic and isotherm studies, Polyhedron 171 (2019) 464–472, https://doi.org/10.1016/j.poly.2019.07.037.
[56] D.R. Rout, H.M. Jena, Removal of malachite green dye from aqueous solution using reduced graphene oxide as an adsorbent, Mater. Today: Proc. 47 (2021) 1173–1182, https://doi.org/10.1016/j.matpr.2021.03.406.
[57] P.K. Boruah, B. Sharma, N. Hussain, M.R. Das, Magnetically recoverable Fe_3O_4/graphene nanocomposite towards efficient removal of triazine pesticides from aqueous solution: Investigation of the adsorption phenomenon and specific ion effect, Chemosphere 168 (2017) 1058–1067, https://doi.org/10.1016/j.chemosphere.2016.10.103.
[58] Y. Sun, X. Liu, Efficient visible-light photocatalytic degradation of imidacloprid and acetamiprid using a modified carbon nitride/tungstophosphoric acid composite induced by a nucleophilic addition reaction, Appl. Surfr. Sci. 485 (2019) 423–431, https://doi.org/10.1016/j.apsusc.2019.04.203.
[59] J. Chen, X. Huang, L. Wang, C. Ma, S. Wu, H. Wang, The synthesis of a dual-template surface molecularly imprinted polymer based on silica gel and its application in the removal of pesticides from tea polyphenols, Anal. Methods 12 (2020) 996–1004, https://doi.org/10.1039/c9ay02708d.
[60] P.T.L. Huong, N. Tu, H. Lan, L.H. Thang, N.V. Quy, P.A. Tuan, N.X. Dinh, V.N. Phan, A.T. Le, Functional manganese ferrite/graphene oxide nanocomposites: effects of graphene oxide on the adsorption mechanisms of organic MB dye and inorganic As(V) ions from aqueous solution, Rsc. Adv. 8 (2018) 12376–12389, https://doi.org/10.1039/c8ra00270c.
[61] H. Du, Y.T. Lei, W.L. Chen, F.C. Li, H.M. Li, W. Deng, G.H. Jiang, Multifunctional magnetic bio-nanoporous carbon material based on zero-valent iron, Angelicae Dahuricae Radix slag and graphene oxide: an efficient adsorbent of pesticides, Arab. J. Chem. 14 (2021) 103267, https://doi.org/10.1016/j.arabjc.2021.103267.
[62] T.R. Zimmer, J.M. Silva, D.H.D.A. Rocha, H.L. Teles, D.S. Barbosa, F.F. Freitas, A.A. Seolatto, Removal of the pesticide methomyl contained in simulated effluent from equipment washing by adsorption in residual orange bagasse, Res. Soc. Dev. 9 (2020). https://doi.org/10.33448/rsd-v9i11.8528.
[63] A. Srikhaow, W. Chaengsawang, T. Kiatsiriroat, P. Kajitvichyanukul, S.M. Smith, Adsorption kinetics of imidacloprid acetamiprid and methomyl pesticides in aqueous solution onto eucalyptus woodchip derived biochar, Minerals 12 (2022) 528, https://doi.org/10.3390/min12050528.
[64] M. Dolatabadi, H. Naidu, S. Ahmadzadeh, A green approach to remove acetamiprid insecticide using pistachio shell-based modified activated carbon; economical groundwater treatment, J. Clean. Prod. 316 (2021) 128226, https://doi.org/10.1016/j.jclepro.2021.128226.
[65] N. Hai, X. Liu, Y.Q. Li, F.Y. Kong, Y.Z. Zhang, S. Fang, Effects of microplastics on the adsorption and bioavailability of three strobilurin fungicides, ACS Omega 5 (2020) 30679–30686, https://doi.org/10.1021/acsomega.0c04787.
[66] A. Kumari, A. Mandal, N. Singh, Kinetics and isotherm modeling of azoxystrobin and imidacloprid retention in biomixtures, J. Environ. Sci. Heal. 54 (2019) 118–128, https://doi.org/10.1080/03601234.2018.1507230.